ARTICLES

$\pi^- p \to \pi^0 \pi^0 n$ near threshold and chiral symmetry breaking

J. Lowe,[1,7] B. Bassalleck,[7] H. Burkhardt,[8] W. J. Fickinger,[5] J. R. Hall,[7] M. D. Hasinoff,[3] D. Horvath,[6,10] G. Koch,[3,*] K. D. Larson,[7,†] J. P. Miller,[2] A.J. Noble,[3,‡] B. L. Roberts,[2] D. K. Robinson,[5] M. Sakitt,[4] M. E. Sevior,[3] N. W. Tanner,[9] C. E. Waltham,[3] T. M. Warner,[2] and D. M. Wolfe[7]

[1]*University of Birmingham, Birmingham, B15 2TT, United Kingdom*
[2]*Boston University, Boston, Massachusetts 02215*
[3]*University of British Columbia, Vancouver, British Columbia, Canada V6T 2A6*
[4]*Brookhaven National Laboratory, Upton, New York 11973*
[5]*Case Western Reserve University, Cleveland, Ohio 44106*
[6]*Central Research Institute for Physics, Budapest, Hungary*
[7]*University of New Mexico, Albuquerque, New Mexico 87131*
[8]*University of Nottingham, Nottingham, NG7 2RD, United Kingdom*
[9]*Oxford University, Oxford, OX1 3RH, United Kingdom*
[10]*TRIUMF, Vancouver, British Columbia, Canada, V6T 2A3*

(Received 12 March 1991)

Total cross sections, angular, and mass distributions for the reaction $\pi^- p \to \pi^0 \pi^0 n$ have been measured for p_{π^-}(lab)=7–140 MeV/c above threshold. The threshold amplitude was used to determine a value for the chiral-symmetry-breaking parameter, ξ, of -0.98 ± 0.52. The $\pi\pi$ scattering lengths a_I for isospin $I=0$ and 2 are derived from this result, together with a current-algebra sum rule. The results are $a_0=(0.207\pm0.028)m_\pi^{-1}$ and $a_2=(-0.022\pm0.011)m_\pi^{-1}$. These values are consistent with chiral symmetry broken by the Weinberg $\pi\pi$ interaction and the effects of the $f_0(975)$ scalar meson.

I. INTRODUCTION

Chiral symmetry is an important feature of elementary-particle dynamics. In the low-energy region, quantum chromodynamics (QCD) becomes nonperturbative and satisfactory calculational methods do not exist. Here chiral symmetry, implemented in the theories of current algebra and the partially conserved axial current, provides a basis for the calculation of many low-energy properties of strongly interacting systems. These methods have been applied extensively to $\pi\pi$ and πN systems and have shown impressive agreement with experiment. In addition, chiral symmetry is of interest in its own right as a rather good fundamental symmetry, relevant to both weak- and strong-interaction physics and relating phenomena in these areas.

Chiral symmetry must be broken to some extent, as is evidenced most directly by the mass of the pion, which would be zero in the chiral limit. However, the details of the chiral-symmetry-breaking terms are not well known (see, for example, the papers by Weinberg [1], Schwinger [2], and Olsson and Turner [3]). The topic is discussed in detail in review articles by Pagels [4], Scadron [5], and Gasser and Leutwyler [6]. Olsson and Turner [3] have shown that, on rather general assumptions, the form of the chiral-symmetry breaking can be characterized for sufficiently low energies by a single parameter ξ. However, there certainly are corrections to their model, and it is not clear at what energies higher-order terms become important.

The nature of chiral-symmetry-breaking terms can be studied by measurements of the $\pi\pi$ scattering amplitudes at zero relative momentum, which vanish in the chiral limit. Experimentally, $\pi\pi$ scattering can only be measured indirectly, for example, by the pion production reactions $\pi N \to \pi\pi N$, which are dominated at low momenta by single-pion exchange. The $\pi\pi$ interaction at zero momentum, where theoretical predictions are least ambiguous, is related to the amplitude for $\pi N \to \pi\pi N$ at threshold, and to be of use, measurements must be made as close to threshold as possible. However, in this region, the yield is low and the detection of outgoing particles is difficult.

A summary of the data available in 1984 is given by Manley [7]. Since Manley's paper appeared, several other measurements have been published or are in progress. The Omicron group have published data for [8–10] $\pi^- p \to \pi^+ \pi^- n$, $\pi^- p \to \pi^- \pi^0 p$, and $\pi^+ p \to \pi^+ \pi^+ n$. Experiments on the channel $\pi^- p \to \pi^+ \pi^- n$ have been carried out at the Paul Scherrer Institute [11] and are in progress at TRIUMF [12]. The channel $\pi^+ p \to \pi^+ \pi^+ n$ has also been studied at TRIUMF [13]. Measurements on $\pi^+ p \to \pi^+ \pi^0 p$ are being carried out at Los Alamos [14]. The present paper reports the first measurements close to threshold for the reaction $\pi^- p \to \pi^0 \pi^0 n$. This channel is the only one with all neutral particles in the final state,

which removes possible ambiguities from Coulomb corrections and enables the outgoing particles to be detected closer to threshold than for charged particles.

II. EXPERIMENTAL METHOD

Since the π^0 decays rapidly to two photons, observation of the $\pi^- p \to \pi^0\pi^0 n$ reaction involves the detection of four γ's from $\pi^- p$ interactions. In the present experiment, this was achieved using a large NaI-detector array. Events from the reaction $\pi^- p \to \pi^0 n$, which has two γ's in the final state, were also recorded. The cross sections for this reaction are well known, and the cross sections for $\pi^0\pi^0 n$ could be obtained most accurately by normalization to those for $\pi^0 n$.

The experiment was carried out at the LESB2 separated beam line of the Brookhaven Alternating Gradient Synchrotron. After passing through two beam-defining counters, a momentum-analyzed π^- beam was incident on a liquid-hydrogen target. The target was 18 cm long $\times$ 20 cm diameter and was located at the center of the "crystal box," a 396-element array of NaI detectors [15,16]. The NaI crystals cover four sides of a cube, providing coverage of approximately 2π sr for detection of γ rays from the target. There are 90 crystals, each $6.3\times6.3\times30.5$ cm, on each of the four faces. An additional nine crystals, $6.3\times6.3\times63.5$ cm, are situated at each corner to catch energy leaking from the faces. The arrangement is shown in Fig. 1. To reject events with charged particles in the final state, two stages of charge-veto detectors were used between the target and the NaI. The first of these was a set of scintillator strips, inside the vacuum vessel, around the outside and downstream end of the target. The second stage consisted of four rectangular scintillators covering the faces of the NaI detectors. Precautions were required to maintain the gain stability of the detector elements. The whole of the crystal box and its phototubes were contained in a thermostatically controlled enclosure. To monitor changes in the phototube gains, flashes from a light pulser were fed via optical fibers to each photocube.

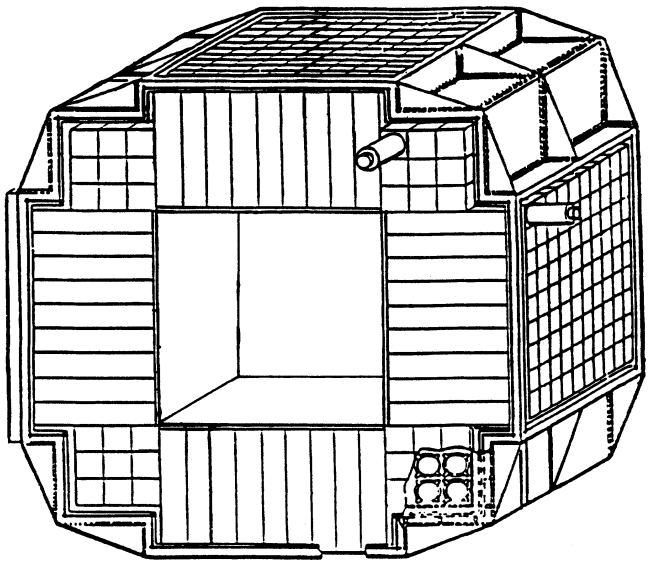

FIG. 1. Arrangement of NaI crystals in the crystal box.

Pulse pileup is a potential hazard, especially with the very low cross sections anticipated near threshold. As a check for pileup, the signal from each NaI-detector element was fed to two analog-to-digital converters (ADC's). One of these was gated with a 200-ns gate to sample the whole of the pulse, while the other sampled the leading portion with a 50-ns gate. During analysis, piled-up pulses were rejected by imposing a condition that pulses in each pair of ADC's be in the correct ratio.

To improve the data-taking rate, LeCroy model 4300 fast encoding and readout ADC's were used, and only ADC's that were at least one channel over pedestal were read out. Further, the data from each event were buffered in two LeCroy CAB preprocessors before being transmitted to the PDP-11 on-line computer. The entire detector, electronic, and data-acquisition setup was quite similar to that used previously for a study of the weak radiative decay of the Λ; this experiment has been described in detail elsewhere [17,18].

In order to record selectively events from the $\pi^- p \to \pi^0\pi^0 n$ reaction in the presence of a much larger event rate from the charge-exchange $\pi^- p \to \pi^0 n$ process, the main trigger required significant energy deposition (at least 30 MeV) in at least three of the four faces of the crystal box. All events satisfying this criterion and producing signals in the beam counters and not in the veto counters were written to tape for analysis off line. An additional trigger, requiring energy in just two faces of the crystal box, recorded charge-exchange events from $\pi^- p \to \pi^0 n$. which were used for normalization of the $\pi^- p \to \pi^0\pi^0 n$ cross section. A sample of about 1% of these events was written to tape.

The beam momentum was determined primarily by the last dipole magnet in the beam line. In addition, a scintillator hodoscope in the beam just upstream of the target measured the beam-particle position in the dispersion plane of this magnet, providing additional momentum analysis of the beam. The field in this dipole was monitored both by measurement of the current and by a Hall probe located in the magnet gap.

Measurements were made for nine field settings of the dipole magnet, one of which corresponded to a momentum below the threshold for $\pi^- p \to \pi^0\pi^0 n$ of 265.7 MeV/c. At each magnet setting, the data were divided into up to five momentum bins according to the momentum determined by the hodoscope. At beam momenta below 300 MeV/c, the momentum difference between consecutive hodoscope sections was about 4 MeV/c. Runs were made at beam momentum settings spaced at intervals of 10 MeV/c, thus providing an overlap in momentum between data from different settings of the dipole magnet. The momentum range from just below threshold to about 410 MeV/c was covered in the experiment. At each momentum setting, runs were also taken with the target empty.

Energy calibration of the NaI-detector elements was determined by observing monoenergetic 129.4-MeV γ

rays from the process $\pi^- p \to \gamma n$ at rest. For this purpose, sufficient Cu degrader was inserted in the π^- beam to cause pions to stop in the liquid-hydrogen target. Two such calibration runs were carried out during the experiment.

III. RESULTS

A. Data analysis

All events were checked off line to ensure that pulses in the beam-line counters corresponded to a single pion, that there was only one particle in the hodoscope, and that there was no signal in any veto counter. In any NaI detector with more than 2.5 MeV, the correct ratio was required for the two ADC signals with different gate widths. Additional checks were applied to time-to-digital converters (TDC's) on each of the beam-line counters and groups of NaI detectors in the crystal box. However, these cuts were redundant since, although out-of-time events were visible in the raw data tapes, none survived the ADC cuts; all were found to be pileup events giving the wrong ratio for at least one pair of NaI ADC's.

A single γ ray typically showers into about six crystals in the crystal box. Therefore, the signals in the individual NaI elements were grouped into "clumps," each clump supposedly corresponding to a single γ ray. The method used to achieve this was derived from a procedure developed at Los Alamos for the crystal box [15,16]. For each event, the highest-pulse-height crystal (HPHC) was searched for. Then the total energy was summed in the group of crystals, called the "neighborhood set," centered on this HPHC. The neighborhood set was chosen so as to include, as far as possible, all crystals into which a single γ ray could shower. For crystals in one of the four faces, not close to an edge, the neighborhood set was taken as the group of 25 crystals centered on the HPHC. When the HPHC was close to a corner or was one of the corner crystals, the neighborhood set was defined in an analogous way to contain the shower. When the HPHC was in an upstream or downstream edge crystal, i.e., an edge crystal not adjacent to a group of corner crystals, no satisfactory neighborhood set could be defined because of loss of energy from the edges of the crystal box. Events containing such a HPHC were rejected.

The total energy in the neighborhood set was taken as a measure of the γ-ray energy. The procedure was repeated by searching for the highest pulse height in crystals not already used in the first neighborhood set. This process was continued until no crystal with more than 5 MeV remained in that event. Reference 16 describes the procedure in more detail.

Our procedure is identical to that used at Los Alamos, except for some minor changes in the definition of the neighborhood set. These changes were suggested by examination of the shower distribution in both data and simulated events.

This method has two obvious limitations. First, if two γ rays are close enough that their neighborhood sets overlap, the method may apportion the energy incorrectly between the two γ rays and may even fail to recognize the presence of the second γ ray. To minimize errors from this source, the rms size of each clump was calculated. Monte Carlo studies showed that this quantity is usually much larger for clumps containing two overlapping γ rays. A cut was therefore applied on the rms clump size during the analysis, which reduced the problem of overlapping clumps to the point where it could be reliably calculated in the Monte Carlo simulation. A second problem with the procedure is that the total energy of a clump is always less than the γ-ray energy, since there is inevitably some energy leakage out of the sides or back of the crystal box. The extent of this leakage depends on the location of the clump in the crystal box, in particular, how close the HPHC is to an edge. Again, this effect was calculated in simulation studies, and based on the results of this, the energy of each clump was corrected to yield the full γ-ray energy.

The spectra from the stopping π^- runs were used to calibrate the gains of all elements of the crystal box. For this purpose, a Monte Carlo program was used to trace the shower development and energy deposition in the NaI resulting from monoenergetic 129.4-MeV γ rays produced in the target by $\pi^- p \to \gamma n$ at rest. The Monte Carlo spectrum for each crystal was then compared with the observed spectrum, and the set of 396 gain parameters was treated as the variable parameters in a least-squares fit of the entire set of spectra. With gains determined this way, the resolution of the crystal box was about 8% full width at half maximum (FWHM) at 129.4 MeV.

The data from the in-flight pion interactions were then analyzed for events with a γ multiplicity of 2 or 4, respectively, for the triggers requiring energy in 2 or ≥ 3 faces of the crystal box. Pairs of γ rays with a mass of a π^0 were then selected and the event missing mass was calculated. To do so requires a knowledge of the vertex position. The lateral vertex position was deduced from the hodoscope information. No information was available on the vertical and longitudinal vertex coordinates, which were therefore taken to be those of the target center. Some spectra of missing masses, after subtraction of target-empty background, are shown in Fig. 2. For the γ-multiplicity-4 events, the missing-mass spectra were exceptionally clean, even close to threshold, and show a clear peak at the neutron mass. Measurements taken at beam momentum settings below threshold showed no events in the neutron-mass region. For the γ-multiplicity-2 events, a significant target-empty background was found, but after subtraction of this target-empty background, the spectra were nevertheless free from events away from the neutron-mass peak. During the analysis, it was found that the acceptance was quite sensitive to the energy threshold used to determine the number of faces of the crystal box containing energy. Therefore, rather than rely on the somewhat unstable cut provided by the hardware discriminator, a threshold of 50 MeV was imposed in the off-line analysis.

Electron contamination of the π^- beam was usually small, but somewhat variable. There was no evidence that electrons could give triggers that satisfied all the cuts on the events. Also, their presence in the beam did not

disturb determination of the absolute cross sections, since this relied only on the ratio of the $\pi^0\pi^0 n$ to $\pi^0 n$ event rates, not on the absolute π^- flux. The only indirect effect of electron contamination was in the relative normalization of the target-full and target-empty runs, which was based on the integrated π^- flux for these runs. Their effect is therefore present in the contribution to the error of the target-empty subtraction.

The crystal box has some sensitivity to neutrons. The neutron detection efficiency has been measured in a separate experiment [17] to be about 6%. This number is too small and not sufficiently well known for neutron detection to be useful in improving the definition of $\pi^0\pi^0 n$ events by requiring that the neutron be identified. In any case, the spectra in Fig. 2 suggest that the events are cleanly identified from the γ's alone. Neutrons are a potential problem in that if a neutron is misidentified as a γ or vice versa, a valid event will be lost because the γ multiplicity will be counted wrongly. Neutrons tend to leave most of their kinetic energy in a single NaI crystal, and a clump was taken to be a neutron if $\geq 95\%$ of the energy was contained in a single crystal. This criterion has been shown to fail to identify a neutron in about 50% of cases. However, the effect of this on the extracted cross sections would be $\leq 4\%$ if the error were ignored. In fact, these properties of neutron and γ clumps are, of course, modeled in the simulation (see below), and so no error would be introduced if the simulation program describes them accurately. In practice, the errors from neutron misidentification are probably reduced to well below 1%.

B. Simulation

The Monte Carlo simulation program GEANT [19] was used to calculate the acceptance of the apparatus. Events were generated in the target volume and reaction products were tracked through all veto counters and other materials into the NaI, where the resulting shower was also tracked. Calculations were made for the signal channel $\pi^- p \to \pi^0\pi^0 n$ and for the normalization channel $\pi^- p \to \pi^0 n$. In addition, the channel $\pi^- p \to \pi^-\pi^0 p$ was simulated because a background source arises from this channel when the π^- stops in liquid hydrogen and the reaction $\pi^- p \to \pi^0 n$ ensues. No simulation of the incident beam was required since the cross sections were deduced from the ratio of two reactions measured in the same run, and so knowledge of the absolute π^- flux was not needed.

The angular distributions for the $\pi^- p \to \pi^0 n$ reaction were taken from the phase-shift analysis SAID of Arndt, Ford, and Roper [20]. For the production reactions $\pi^- p \to \pi^0\pi^0 n$ and $\pi^- p \to \pi^-\pi^0 p$, angular distributions were taken to be isotropic in the center of mass for the neutron and isotropic in their rest frame for the two pions, and the mass distributions were taken to follow phase space between the kinematically allowed limits.

It was found that the acceptance was quite insensitive ($\leq 1\%$) to the lateral position of the beam particle on the target. Therefore, it was not necessary to model the beam-spot shape with any great accuracy. However, the missing-mass resolution was found to depend on the beam-spot shape, and as a result, different missing-mass cuts were needed in the data and simulation spectra. The acceptance is not sensitive to these cuts provided they are set wide enough to include all events.

An experimental problem arose in that the efficiency of the veto counters surrounding the target was not well known. These counters had long, thin light guides and the efficiency may have fallen below 100%, especially at the ends. It was found that the acceptance for $\pi^- p \to \pi^0 n$ and $\pi^0\pi^0 n$ did not depend significantly on the

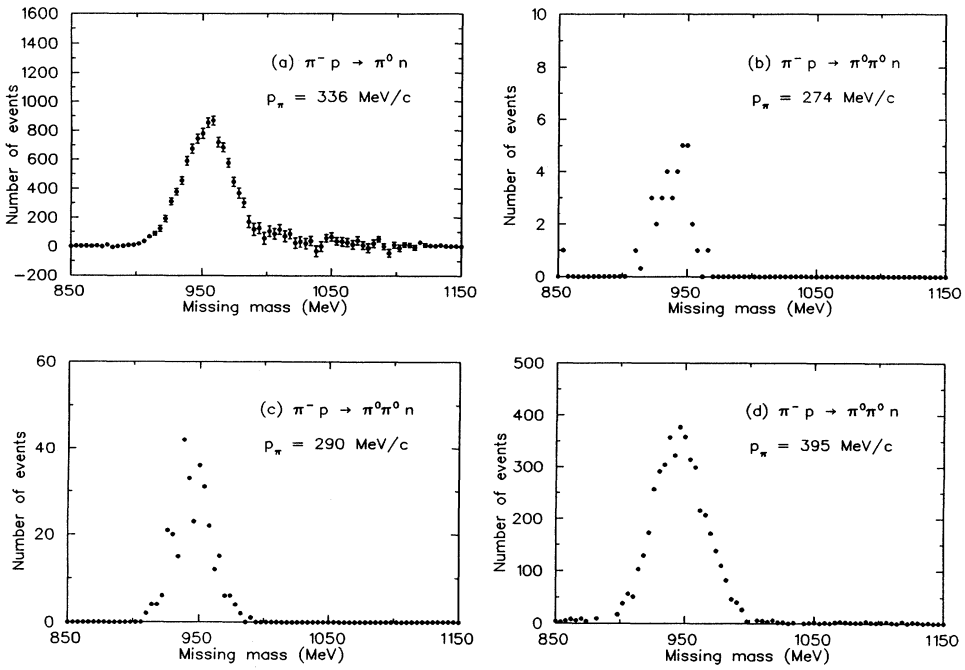

FIG. 2. Missing-mass spectra for (a) $\pi^- p \to \pi^0 n$ and (b)–(d) $\pi^- p \to \pi^0\pi^0 n$ at various momenta.

efficiency of these counters, but that for $\pi^- p \to \pi^- \pi^0 p$ did. The correction of the cross section for contamination from this reaction varies with beam momentum between 0% and 3%. We take the cautious view that the veto counters operate with 100% efficiency, but take the difference in the derived cross sections for 0% and 100% efficiency as the uncertainty from this source of background.

The acceptance was found to depend sensitively on the energy threshold for the summed energy in each face, used to determine how many faces of the crystal box contained energy. Raising this threshold above 50 MeV caused the numbers of both simulated and data events to fall. Even when each of these numbers changed by a significant factor, the ratio of them remained constant within the statistical accuracy. We conclude that the effect of this threshold is accurately described by the simulation.

As mentioned above, the $\pi^- p \to \pi^0 \pi^0 n$ events were generated assuming isotropic angular distributions and phase-space mass distributions. The data depart from this assumption in one important respect: There is a pronounced enhancement in the $m_{\pi\pi}$ spectrum at high $\pi\pi$ masses, especially at high beam momenta (see Sec. III D and Fig. 5). For beam momenta above about 320 MeV/c, this effect is sufficiently strong to affect the calculated acceptance, and it was necessary to weight the Monte Carlo events to fit the observed $m_{\pi\pi}$ spectrum. The effect of this on the acceptance is negligible for beam momenta below 320 MeV/c and rises to reach 12% at 400 MeV/c. Various weighting functions were tried. The calculated acceptance did not depend on the functional form provided it reproduced, at least approximately, the observed $m_{\pi\pi}$ spectrum. The overall acceptance found for $\pi^- p \to \pi^0 \pi^0 n$ varied from $\sim 5\%$ at threshold to $\sim 1.5\%$ at the highest momentum studied.

C. Beam momentum

Since the cross section varies rapidly with incident momentum near threshold, an accurate determination of the beam momentum is important. Calculations were made using the Monte Carlo program DECAY TURTLE [21], which traces the trajectories of particles through beam-line elements. The positions and fields of all elements from the production target to the hydrogen target were set to the values used during the experiment. The effects were then studied of displacing all beam-line elements *except* the final dipole $D2$ from the surveyed positions and measured currents. Changes of $\geq 5\%$ in current, ≥ 10 cm in longitudinal position, and 2.5 cm in lateral position were investigated. All of these displacements are much greater than the accuracy with which the positions and fields are known. The results showed that, in all cases, the change in calculated beam momentum was $\leq 0.3\%$. To this accuracy, therefore, the beam momentum depends only on the effective length and central field of $D2$.

DECAY TURTLE was also used to determine the momentum dispersion of $D2$ and hence the momentum as a function of beam position on the hodoscope. The dispersion was found to be similarly insensitive to the settings of the beam-line elements.

During the running, this field was monitored with a Hall probe and the current was measured. After the run, a NMR probe was installed at the center of the magnet and the field was measured for a series of currents. The relationships between the field, current, and Hall voltage were found to be linear and reproducible to about 0.2%, and a repeat of this calibration 6 months later established the long-term stability to be better than 0.1%.

The effective length of $D2$ had been measured in earlier experiments from magnetic-field measurements [22] and also during Brookhaven experiment E701 [23] in which the range of a pion beam that had been momentum analyzed by $D2$ was measured. These two determinations gave effective lengths of 87.9±0.9 and 87.8±0.9 cm, respectively.

These data enable the beam momentum to be determined to about 1%. In fact, the behavior near threshold of the cross sections measured in the present experiment provides an additional determination of the beam momentum. As described below (Sec. IV B), this turns out to be consistent with the two previous determinations and improves on the accuracy.

Because of the rapid variation of cross section with momentum, not only the mean beam momentum, but

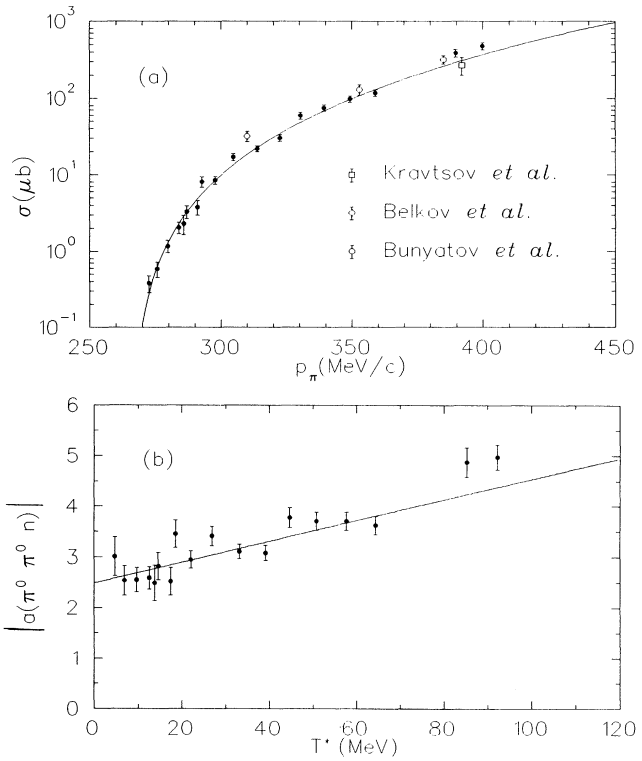

FIG. 3. (a) Cross section from the present experiment for $\pi^- p \to \pi^0 \pi^0 n$ as a function of laboratory π^- momentum. Also shown are the data of Kravtsov *et al.* [25], Belkov *et al.* [26], and Bunyatov *et al.* [27]. In addition to the errors shown, there is an overall scaling error of ±6%. The curve is a fit to all points below $p_{\pi^-} = 380$ MeV/c of phase space and an amplitude linear in total center-of-mass energy. (b) The experimental amplitudes and the fitted amplitude linear in T^*.

also the momentum profile is important in interpreting the results. The momentum profile of the beam leaving $D2$ was calculated using DECAY TURTLE. This was combined with the momentum loss to the target center and the momentum spread due to the target thickness to yield the overall momentum profile.

D. Cross sections

The cross sections were extracted from the numbers of events in the missing-mass plots such as those in Fig. 2, together with the prescale factors, the known cross sections for $\pi^- p \to \pi^0 n$ measured by Bugg *et al.* [24], and the acceptances calculated from the simulation program. For each setting of the $D2$ field, the data could be separated into ten different beam momenta corresponding to the ten elements of the beam hodoscope. In fact, data from several hodoscope sections were combined in such a way as to provide more closely spaced points in the region where the cross section changes most rapidly. The calculated contribution from $\pi^- p \to \pi^- \pi^0 p$ (see Sec. III B) was subtracted from the data. This correction is negligible at the lowest and highest momenta and reaches a maximum of 3% at about 300 MeV/c. The threshold for $\pi^- \pi^0 p$ is 4.5 MeV higher than that for $\pi^0\pi^0 n$, and so this background is zero at the lowest-momentum point measured.

Since the cross section varies over the range of momenta spanned by the beam momentum resolution and target thickness, the effective momentum was calculated for each data point. The effective momentum is defined as the momentum of a monoenergetic beam which would have the same cross section as for the actual momentum profile. Thus, if the experimental momentum distribution is $f(p)$, the effective momentum p_{eff} is given implicitly by

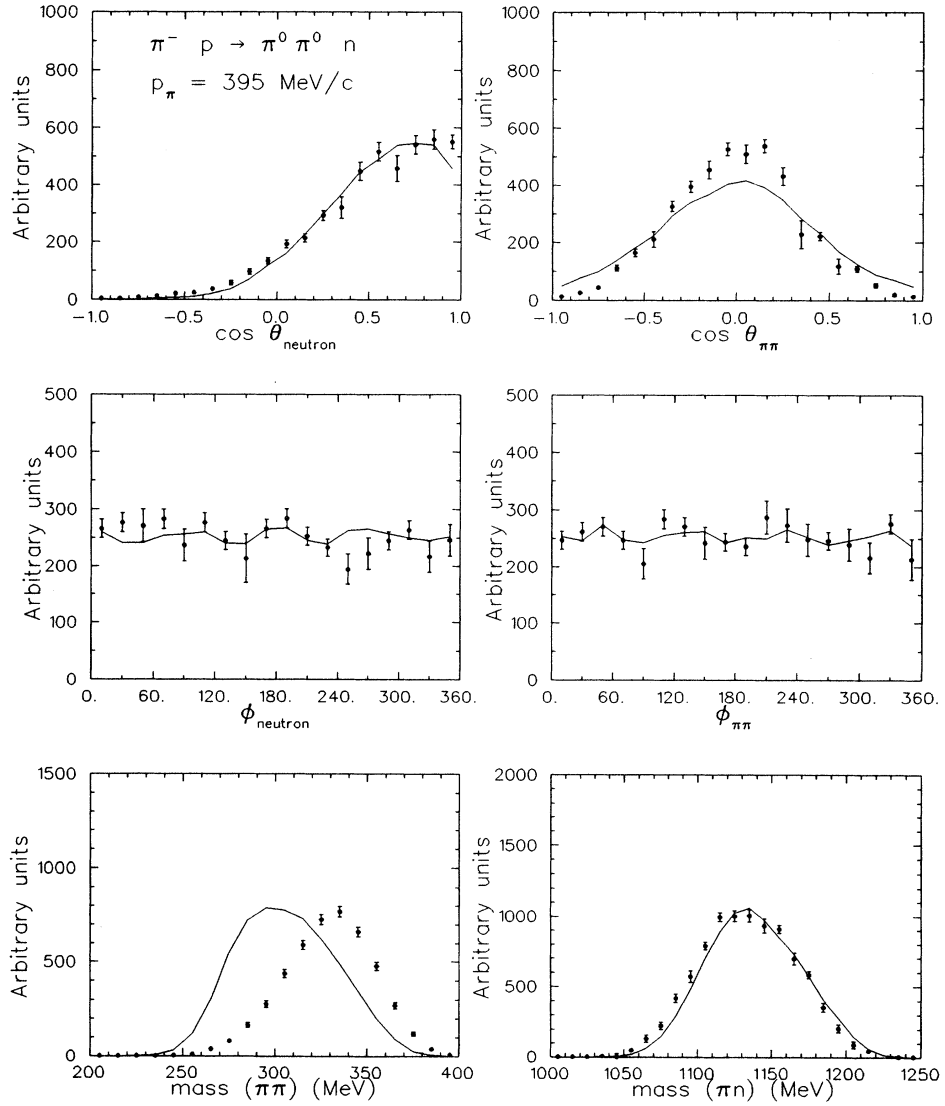

FIG. 4. Dependence of the $\pi^- p \to \pi^0\pi^0 n$ yield on neutron and $\pi^0\pi^0$ angular coordinates and on $\pi^0\pi^0$ and $\pi^0 n$ masses for the summed data at $p_{\pi^-} = 390$–400 MeV/c. The curves are predictions of simulation calculations (see text).

$$\sigma(p_{\text{eff}})=\frac{\int f(p)\sigma(p)dp}{\int f(p)dp} .$$

Obviously, this is an iterative process since to calculate p_{eff} the momentum dependence of the cross section must already be known. However, this momentum dependence is given mainly by phase space and known kinematic factors, especially near threshold. In the next section, we show that there is, in addition, a mild momentum dependence of the amplitude; this was included in the evaluation of the integral. Fortunately, this momentum dependence is so weak that a single iteration is adequate.

The cross sections are shown in Fig. 3(a) and are listed in Table I. The errors shown are statistical, together with such nonstatistical errors that vary with momentum. These arise mainly from uncertainties in the target-empty subtraction ($\leq 5\%$), the acceptance ($\leq 5\%$), and the veto counter efficiency ($\leq 3\%$). Uncertainties in the cross section for $\pi^- p \to \pi^0 n$ from interpolating in the data of Ref. [24] contribute up to 3%. In addition, there is an overall systematic error of 6%, not included in Fig. 3(a), which

TABLE I. Cross sections from the present experiment for $\pi^- p \to \pi^0 \pi^0 n$. The cross sections given are subject to an additional systematic error of ±6%.

Beam momentum (MeV/c)	Cross section (μb)
272.5	0.382±0.096
275.5	0.59±0.14
279.7	1.18±0.22
283.9	2.06±0.35
286.9	3.33±0.64
285.7	2.31±0.65
291.0	3.81±0.81
292.6	8.1±1.3
297.7	8.5±1.0
304.7	17.1±1.9
313.8	21.9±2.0
322.5	30.3±3.0
330.5	59.8±6.4
339.4	75.2±7.3
349.4	98.1±9.3
359.1	118±11
389.6	388±46
399.9	479±49

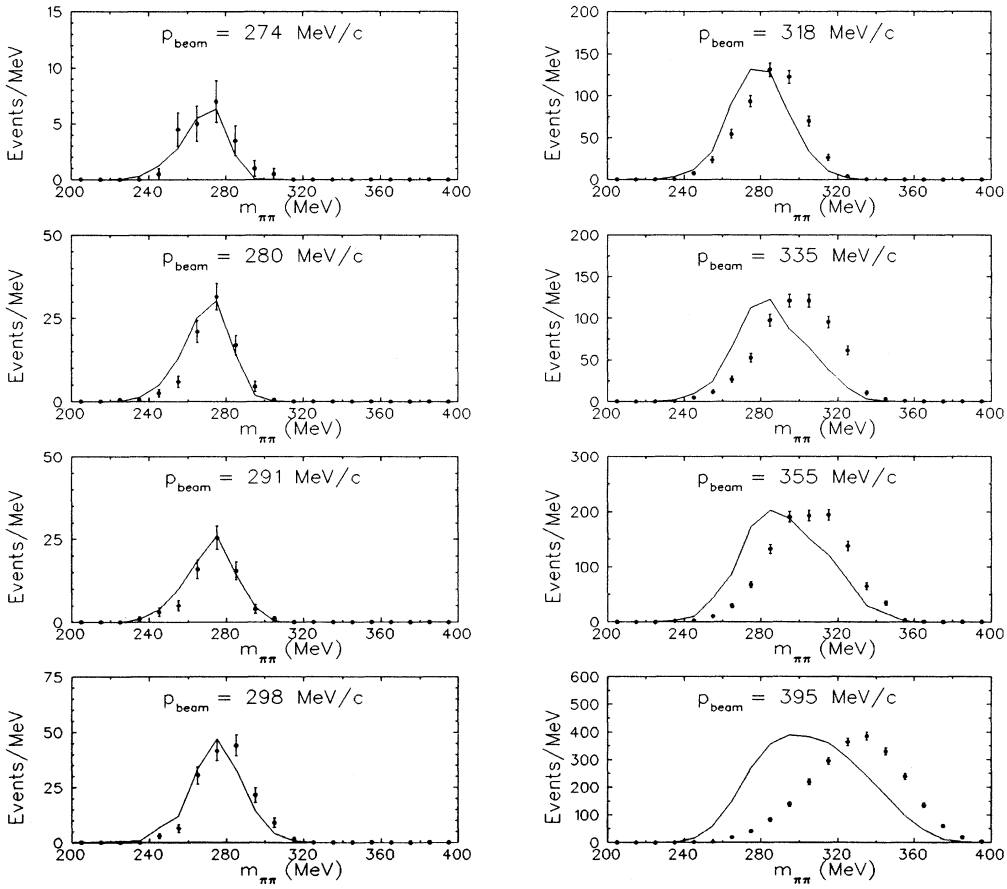

FIG. 5. Data (points) and simulation predictions (curves) for $m_{\pi\pi}$ at various incident π^- momenta.

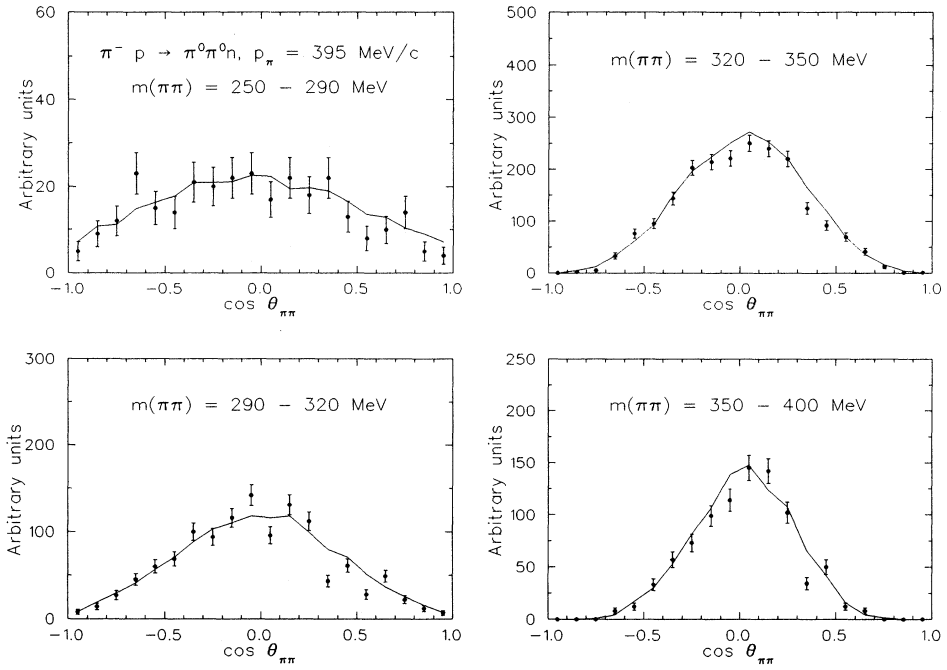

FIG. 6. Comparison of data (points) and simulation (curves) for $\cos(\theta_{\pi\pi})$ for four ranges of $m_{\pi\pi}$, showing the dependence of the acceptance for $\cos(\theta_{\pi\pi})$ on $m_{\pi\pi}$.

arises mainly from uncertainties in the cuts on mass spectra and in the sampling factor for the charge-exchange events.

Also shown in Fig. 3(a) are four data points from previous work [25–27] below 400 MeV/c. The agreement is good and the present data extend much closer to threshold than earlier work. The lowest point in Fig. 3(a) is within 5 MeV in total center-of-mass energy of threshold.

The dependence of the cross section on other kinematic variables is illustrated in Fig. 4. The yield is plotted as a function of angles of the neutron (θ_n, ϕ_n) in the overall center of mass, the $\pi^0\pi^0$ relative motion in the $\pi^0\pi^0$ rest frame, and the $\pi^0\pi^0$ and $\pi^0 n$ invariant masses. The data plotted in Fig. 4 are the combined data from the two highest-momentum points in Fig. 3(a). The curves in Fig. 4 show the predictions of simulation calculations in which the events were generated with isotropic angular distributions and phase-space mass distributions. The angular distribution curves therefore represent the acceptance of the apparatus. All variables are well fitted by these simulations except for the $\pi^0\pi^0$ mass, for which the data are displaced toward higher masses. Similar plots for lower beam momenta show the same characteristics except that the enhancement at high $\pi^0\pi^0$ masses is less. This is illustrated in Fig. 5, where the data and simulation for $m_{\pi\pi}$ are compared for a range of beam momenta. Apart from the $m_{\pi\pi}$ distribution, the data are consistent, over the range covered by the experimental acceptance, with the isotropic angular distributions and phase-space mass distributions assumed in the simulation.

The apparent discrepancy in Fig. 4 between the $\cos(\theta_{\pi\pi})$ distributions for data and simulation is not real, but is a consequence of the dependence of the acceptance on $m_{\pi\pi}$ and the fact that the data do not follow the phase-space $m_{\pi\pi}$ distribution used in the simulation. The dependence on $m_{\pi\pi}$ is shown in Fig. 6, where the $\cos(\theta_{\pi\pi})$ distribution of Fig. 4 is separated into four ranges of $m_{\pi\pi}$ and each is compared with simulation for the corresponding range. The agreement for each range of $m_{\pi\pi}$ is good.

IV. INTERPRETATION OF THE DATA

A. $\pi^0\pi^0$ mass spectrum

The enhancement seen in the $\pi^0\pi^0$ mass spectrum shown in Fig. 5 has been observed previously [8] in the $\pi^+\pi^-$ channel, but not in the $\pi^-\pi^0$ or $\pi^+\pi^+$ channels [9,10]. Thus the effect presumably has isospin $I=0$. At first sight, the effect is suggestive of $\pi\pi$ resonance with a mass of about 400 MeV. However, no set of resonance parameters could be found which fit the data with a single resonance plus a phase-space contribution; the mass extracted from such a fit appears to vary with the incident π^- momentum. Exactly the same effect was found in several previous studies, for example, by Saxon, Mulvey, and Chinowsky [28] in their study of $\pi^- p \to \pi^+\pi^- n$ at 450–550 MeV/c. They analyzed their data with a model which includes a parametrized form of the $\pi\pi$ phase shift together with $\pi\pi$ and πN resonances. They found good fits to all measured kinematic variables including the $\pi^+\pi^-$ mass spectra. However, they emphasize that the observed enhancement is not directly a resonance, but arises from other effects, in particular the peculiar behavior of the s-wave $\pi\pi$ phase shift.

It is tempting to associate the enhancement with the

$J^P=0^+$ σ meson which forms a basic ingredient of the σ model as a realization of chiral symmetry [4,5]. The σ meson may well be responsible for the rather large $\pi\pi$ phase shift at $\sim$100–200 MeV above threshold. However, although it may have a significant effect on the $\pi\pi$ mass spectrum, the width predicted and, apparently, observed [29] for the σ meson is far too large to generate by itself the observed behavior.

We conclude that this enhancement is not directly relevant to the chiral-symmetry properties of the $\pi\pi$ system.

B. Total cross sections

From the point of view of chiral symmetry, the most important quantity to be extracted from the total cross sections is the amplitude at threshold. To do this, we approximate the three-body phase space by treating the final-state particles nonrelativistically. The total cross section then takes the form

$$\sigma=24.994\frac{QT^{*2}}{W^2}|a(\pi^0\pi^0n)|^2S ,$$

where Q is the center-of-mass momentum of the incident π^-, W is the total center-of-mass energy, and T^* is the total center-of-mass kinetic energy in the final state. The dimensionless amplitude is $a(\pi^0\pi^0n)$ and $S=\frac{1}{2}$ is a statistical factor resulting from the identity of the final-state pions. With Q, W, and T^* in MeV, σ is in microbarns.

The momentum dependence of the amplitude $|a(\pi^0\pi^0n)|$ cannot be predicted on general grounds. Previous analyses [7–10] of $\pi p\to\pi\pi N$ data have taken a to be either constant or linear in T^* or quadratic in $\sqrt{T^*}$. There has been no convincing evidence for any momentum dependence other than linear in T^* and, hence, in the total center-of-mass energy W. Initially, therefore, the present data were fitted with the linear form

$$|a(\pi^0\pi^0n)|=|a_0(\pi^0\pi^0n)|+bT^* ,$$

for the amplitude. Since errors in the beam momenta would cause a bad fit near threshold, all beam momenta were scaled by a common factor which was varied in the fit. It was found that the two highest-momentum points contributed unduly to the χ^2 for the fit. This is presumably a result of inadequacy of the linear form for $|a(\pi^0\pi^0n)|$. Since the main object of fitting the data was to extract the threshold amplitude, these highest two points were dropped from the fit, thus reducing the χ^2 by 4.4.

The fit gave a χ^2 of 19.2 for 16 data points and 3 varied parameters. The fitted amplitude is plotted as a function of T^* in Fig. 3(b), which also shows the experimental points after the phase-space and kinematic factors have been divided out. The fitted value of the momentum scaling factor gives an effective length for the $D2$ magnet of 88.5±0.3 cm, which is consistent with the previously measured values (see Sec. III C).

The fitted value of the threshold amplitude is

$$|a_0\pi^0\pi^0n)|=2.45\pm0.16 .$$

The sign of $a_0(\pi^0\pi^0n)$ cannot be deduced from the data. Other parametrizations were tried for $a(\pi^0\pi^0n)$ as a function of momentum, including terms in $\sqrt{T^*}$ and W^2. None of these parametrizations gave as good a fit (in terms of χ^2/degree of freedom) as the linear fit, and the values for the threshold amplitudes from all these parametrizations were reasonably consistent. Further, a linear extrapolation to threshold is appropriate [1,30] for extraction of the $\pi\pi$ scattering lengths. Therefore, we adopt the above value as the threshold amplitude for $\pi^-p\to\pi^0\pi^0n$.

Olsson and Turner [3] showed that, using an almost model-independent chiral Lagrangian, the effect of the chiral-symmetry-breaking terms on threshold pion production can be described by a single parameter ξ, and they derive an expression for the threshold amplitude in terms of ξ. Evaluation of this expression requires values for the coupling constant $G_{NN\pi}$ and for the combination $(M_{\text{nucleon}}/G_{NN\pi})(g_A/g_V)$, which is related by the Goldberger-Treiman relation to the pion decay constant f_π. Recent values for the parameters involved have been discussed by Coon and Scadron [31]. They point out that if values for $G_{NN\pi}$, g_A, and M_{nucleon} are evaluated at the chiral limit, the Goldberger-Treiman relation gives $f_\pi=90.1$ MeV, whereas the standard (on-shell) values give 88.4 MeV. By comparison, the experimental value of f_π is 92.6 MeV. There is no obviously correct value to use for f_π in this context, but we take the view that using the value $f_\pi=90.1$ MeV, evaluated at the chiral limit, is appropriate for the present analysis. Chiral-symmetry breaking is then included explicitly using the model of Olsson and Turner.

The threshold amplitude for the $\pi^-p\to\pi^0\pi^0n$ reaction can be related to ξ through the expression [3,32]

$$a_0(\pi^0\pi^0n)=2.149-0.307\xi .$$

With our experimental value for $|a_0(\pi^0\pi^0n)|$, we find $\xi=-0.98\pm0.52$, choosing the positive sign for $a_0(\pi^0\pi^0n)$, or $\xi=-15.0\pm0.5$ for the negative sign.

No other experiment on $\pi^-p\to\pi^0\pi^0n$ has produced data sufficiently close to threshold to enable a value of ξ to be extracted. Several experiments on other charge states have yielded results for ξ. These are not particularly consistent among themselves, but in general the values of ξ are around zero or slightly negative. To this extent, the present result, with the positive sign for $a_0(\pi^0\pi^0n)$ is consistent with most earlier experiments, but the negative sign for $a_0(\pi^0\pi^0n)$ is excluded. One experiment that differs from this is the Omicron result [10] for $\pi^+p\to\pi^+\pi^+p$, which gave $\xi=1.56\pm0.26\pm0.39$. However, this is not consistent with other data [13] on the same channel, which gave $\xi=-0.20\pm0.15$. The result obtained for ξ from a $\pi N\to\pi\pi N$ experiment, however, depends not only on the data, but also on the procedure used to extrapolate to threshold. Also, the extraction of ξ is sensitive to the choice of parameters and several different approaches have been used in the past. A more meaningful interpretation would result from a simultaneous analysis of data from all channels on a consistent basis. An analysis along these lines is in progress [33].

Olsson and Turner [3] showed that the value of ξ is re-

lated to the s-wave $\pi\pi$ scattering lengths, a_I, for $I=0$ and 2, by

$$\frac{a_2}{a_0}=\frac{\xi+2}{\frac{5}{2}\xi-7} .$$

This relation, together with our value for ξ, can be combined with the current-algebra sum rule [1,30,34]

$$2a_0-5a_2=\frac{3m_\pi}{4\pi f_\pi^2}=0.526m_\pi^{-1} ,$$

to give values for the $\pi\pi$ scattering lengths. This procedure gives

$$a_0=(0.207\pm0.028)m_\pi^{-1} ,$$

$$a_2=(-0.022\pm0.011)m_\pi^{-1} .$$

One of the earliest calculations of these scattering lengths is the current-algebra work of Weinberg [1]. Weinberg's $\pi\pi$ interaction corresponds to a value for ξ of zero. However, it has been pointed out by Jacob and Scadron [34] that there is an important correction to Weinberg's calculation from the contribution of the $f_0(975)$ scalar meson. They argue that the $f_0(975)$ is the most significant contributor since the σ meson is already implicitly included in their chiral Lagrangian and the effect of its radial excitation, the $f_0(1400)$, is small. Taking just the $f_0(975)$, then, Jacob and Scadron show that the addition of this contribution changes the s-wave $\pi\pi$ scattering lengths from Weinberg's values of $a_0=0.156m_\pi^{-1}$, $a_2=-0.045m_\pi^{-1}$ to $a_0=0.201m_\pi^{-1}$, $a_1=-0.028m_\pi^{-1}$. These are in excellent agreement with the present experimental result.

Thus we conclude that our results are in good agreement with chiral symmetry broken by the Weinberg $\pi\pi$ interaction together with the contribution from the $f_0(975)$.

ACKNOWLEDGMENTS

The authors are grateful to M. D. Scadron and L. Turner for many valuable discussions, E. K. McIntyre for work on the data-acquisition software, and G. Garvey and C. M. Hoffman for loan of the crystal box. We are also grateful to R. Meier for maintenance of the hydrogen target, P. Pile for providing the momentum-dispersed beam-line tune, and R. K. Adair and T. L. Trueman for providing the facilities of Brookhaven Laboratory. This work was supported by the U.S. DOE, the NSF, the U.K. SERC, and the Canadian NSERC.

*Present address: DuPont Co., Germany.
†Present address: Center for Naval Analyses, Alexandria, VA 22302.
‡Present address: EP Division, CERN, Geneva 23, Switzerland.

[1] S. Weinberg, Phys. Rev. Lett. **17**, 616 (1966); **18**, 507 (1967); Phys. Rev. **166**, 1568 (1968).
[2] J. Schwinger, Phys. Lett. **24B**, 473 (1967).
[3] M. G. Olsson and L. Turner, Phys. Rev. Lett. **20**, 1127 (1968); Phys. Rev. **181**, 2141 (1969); Phys. Rev. D **6**, 3522 (1972).
[4] H. Pagels, Phys. Rep. **16C**, 219 (1975).
[5] M. D. Scadron, Rep. Prog. Phys. **44**, 213 (1981).
[6] J. Gasser, Ann. Phys. (N.Y.) **136**, 62 (1981); J. Gasser and H. Leutwyler, *ibid.* **158**, 142 (1984).
[7] D. M. Manley, Phys. Rev. D **30**, 536 (1984).
[8] G. Kernel *et al.*, Phys. Lett. B **216**, 244 (1989).
[9] G. Kernel *et al.*, Phys. Lett. B **225**, 198 (1989).
[10] G. Kernel *et al.*, Z. Phys. C **48**, 201 (1990).
[11] R. Baran *et al.*, PSI progress report, 1989; H-W. Ortner *et al.*, Phys. Rev. Lett. **64**, 2759 (1990).
[12] M. E. Sevior *et al.*, TRIUMF experiment E561, 1990 (unpublished).
[13] M. E. Sevior *et al.*, Phys. Rev. Lett. **66**, 2569 (1991).
[14] D. Pocanic *et al.*, Los Alamos proposal E1179, 1990 (unpublished).
[15] S. L. Wilson *et al.*, Nucl. Instrum. Methods A **264**, 263 (1988).
[16] S. L. Wilson, Ph.D. thesis, Stanford University, Los Alamos National Laboratory, Report No. LA-10471-T, 1985.
[17] K. D. Larson, Ph.D. thesis, University of New Mexico, 1990.
[18] A. J. Noble, Ph.D. thesis, University of British Columbia, 1990.
[19] R. Brun, F. Bruyant, M. Maire, A. C. McPherson, and P. Zanarini, GEANT, CERN report, 1986 (unpublished).
[20] R. A. Arndt, J. M. Ford, and L. D. Roper, Phys. Rev. D **32**, 1085 (1985).
[21] K. L. Brown and C. Iselin, CERN Report No. 74-2, 1974 (unpublished).
[22] J. M. Snow, Ph.D. thesis, Yale University, 1983.
[23] E. Jastrzembski, N. Haik, W. K. McFarlane, M. A. Mandelkern, D. C. Schultz, C. Amsler, C. C. Herrman, and D. M. Wolfe, Phys. Rev. D **23**, 2784 (1981); D. C. Schultz, Ph.D. thesis, University of California at Irvine, 1981.
[24] D. V. Bugg, P. J. Bussey, D. R. Dance, A. R. Smith, A. A. Carter, and J. R. Williams, Nucl. Phys. **B26**, 588 (1971).
[25] A. V. Kravtsov, A. V. Kuptsov, L. L. Nemenov, E. A. Starchenko, and D. M. Khazins, Yad. Fiz. **20**, 942 (1974) [Sov. J. Nucl. Phys. **20**, 500 (1975)].
[26] A. A. Belkov, S. A. Bunyatov, B. Zh. Zalikhanov, V. S. Kurbatov, and A. Khalbaev, Yad. Fiz. **28**, 1275 (1978) [Sov. J. Nucl. Phys. **28**, 657 (1978)].
[27] S. A. Bunyatov, G. V. Zholobov, B. Zh. Zalikhanov, V. S. Kurbatov, M. M. Musakhanov, A. Khalbaev, and V. A. Yarba, Yad. Fiz. **25**, 325 (1977) [Sov. J. Nucl. Phys. **25**, 177 (1977)].
[28] D. H. Saxon, J. H. Mulvey, and W. Chinowsky, Phys. Rev. D **2**, 1790 (1970).
[29] S. Weinberg, Phys. Rev. Lett. **65**, 1177 (1990).
[30] M. D. Scadron (unpublished).
[31] S. A. Coon and M. D. Scadron, Phys. Rev. C **42**, 2256 (1990).
[32] L. Turner, Ph.D. thesis, University of Wisconsin, 1969.
[33] J. Lowe and H. Burkhardt, paper presented at the Fourth Conference on the Intersections between Particle and Nuclear Physics, Tucson, Arizona, 1991 (unpublished).
[34] R. J. Jacob and M. D. Scadron, Phys. Rev. D **25**, 3073 (1982).